Water Permeation through Nafion Membranes: The Role of Water Activity

ARTICLE *in* THE JOURNAL OF PHYSICAL CHEMISTRY B · DECEMBER 2008

Impact Factor: 3.3 · DOI: 10.1021/jp804197x · Source: PubMed

3 AUTHORS:

Paul Majsztrik
Liquid Light, Inc.
17 PUBLICATIONS **720** CITATIONS
SEE PROFILE

Andrew B. Bocarsly
Princeton University
202 PUBLICATIONS **6,503** CITATIONS
SEE PROFILE

Jay Benziger
Princeton University
313 PUBLICATIONS **8,146** CITATIONS
SEE PROFILE

THE JOURNAL OF PHYSICAL CHEMISTRY B

Article

Water Permeation through Nafion Membranes: The Role of Water Activity

Paul Majsztrik, Andrew Bocarsly, and Jay Benziger

J. Phys. Chem. B, **2008**, 112 (51), 16280-16289• DOI: 10.1021/jp804197x • Publication Date (Web): 21 November 2008

Water Permeation through Nafion Membranes: The Role of Water Activity

Paul Majsztrik,[†] Andrew Bocarsly,[†] and Jay Benziger*[,‡]

Princeton University, Princeton, New Jersey 08544

Received: May 12, 2008; Revised Manuscript Received: October 17, 2008

The permeation of water through 1100 equivalent weight Nafion membranes has been measured for film thicknesses of 51−254 μm, temperatures of 30−80 °C, and water activities (a_w) from 0.3 to 1 (liquid water). Water permeation coefficients increased with water content in Nafion. For feed side water activity in the range $0 < a_w < 0.8$, permeation coefficients increased linearly with water activity and scaled inversely with membrane thickness. The permeation coefficients were independent of membrane thickness when the feed side of the membrane was in contact with liquid water ($a_w = 1$). The permeation coefficient for a 127 μm thick membrane increased by a factor of 10 between contacting the feed side of the membrane to water vapor ($a_w = 0.9$) compared to liquid water ($a_w = 1$). Water permeation couples interfacial transport across the fluid membrane interface with water transport through the hydrophilic phase of Nafion. At low water activity the hydrophilic volume fraction is small and permeation is limited by water diffusion. The volume fraction of the hydrophilic phase increases with water activity, increasing water transport. As $a_w \rightarrow 1$, the effective transport rate increased by almost an order of magnitude, resulting in a change of the limiting transport resistance from water permeation across the membrane to interfacial mass transport at the gas/membrane interface.

Introduction

The uptake and transport of water in the membranes of PEM fuel cells is essential to their operation,[1−7] affecting both steady state and dynamic response. Membrane hydration is required for high proton conductivity. Water enters the membrane from either from humidified feeds or from product water generated at the cathode and diffuses through the membrane from high concentration to low. Since Nafion has long been the most common membrane material used in PEM fuel cells, numerous investigators have studied water uptake and water transport in Nafion.[1,2,5,7,8] The focus of those studies was to determine values for the diffusion coefficient of water in Nafion. Values reported for the diffusivity of water in Nafion vary depending on experimental technique with values spanning over 3 orders of magnitude at a given temperature. We recently demonstrated that interfacial mass transport resistances and polymer swelling are often the limiting resistances to water transport in Nafion.[1,9]

The three most common techniques used to study water transport in Nafion are mass uptake, NMR relaxation, and water permeation. Most studies have assumed diffusion is the limiting resistance to water transport and calculated diffusion coefficients from the measured transport rates. Diffusivity determined by NMR measurements[10−13] gives the highest values of diffusivity ($\sim 10^{-6}$ cm^2/s); permeation and water desorption measurements[11,14−16] give intermediate values of water diffusivity ($\sim 10^{-7}$ cm^2/s); and water sorption measurements[2,11,14,17−23] give the smallest diffusion coefficients ($\sim 10^{-8}$ cm^2/s). However, these three techniques do not capture the same information about water transport.

NMR relaxation determines the self-diffusion of water in Nafion. This technique only considers the motion of water within the fraction of the membrane occupied by water and does not include the influence of the volume fraction of the polymer through which water is transported. As a result, values for D determined by NMR should be reduced to account for membrane structure when scaling to macroscopic transport.

Mass uptake experiments involve monitoring the mass of a Nafion membrane or film as it either sorbs or desorbs water. Mass uptake involves interfacial mass transport at the membrane interface, water diffusion in the Nafion, a solvation reaction between sulfonic acid and water, as well as swelling and relaxation of the polymer network. The technique is dynamic, with properties changing as a function of time. As a result, mass uptake is complicated and is not useful for determining diffusivity unless all aspects of transport are considered and carefully modeled.[1,9] Several investigators have wrongly assumed Fickian water sorption dynamics, leading to erroneous estimations of water diffusivity in Nafion.[17,18,24]

We focus here on water permeation through Nafion. Permeation experiments closely approximate the transport of water into and through the membrane occurring in an operating fuel cell; mass transport at the membrane interfaces as well as diffusion through the membrane are present during steady state permeation. Experiments were designed to measure water permeation through Nafion from vapor feeds of different activity, as well as from liquid water. Permeation was measured as a function of water activity and temperature. Different membrane thicknesses were tested in order to separate interfacial mass transport resistance from diffusion resistance. Finally, permeation through a bilayer of Nafion and a porous carbon sheet or gas diffusion layer (GDL) was investigated.

Experimental Section

Materials. Extruded Nafion films with 1100 EW were purchased from Ion Power: N112 (50.7 μm dry thickness), N115 (127 μm dry thickness), and N1110 (254 μm dry thickness) (Ion Power, New Castle Delaware, USA). Nafion films were treated following the standard cleaning procedure: boil 1 h in 3% H_2O_2 solution, boil 1 h in deionized (DI) water, boil 1 h in 0.5 M sulfuric acid, boil 1 h in DI water twice. While still wet, the polymer was cut into squares 2.5 cm on a side. Nafion

* benziger@princeton.edu
[†] Department of Chemistry.
[‡] Department of Chemical Engineering.

10.1021/jp804197x CCC: $40.75
Published on Web 11/21/2008

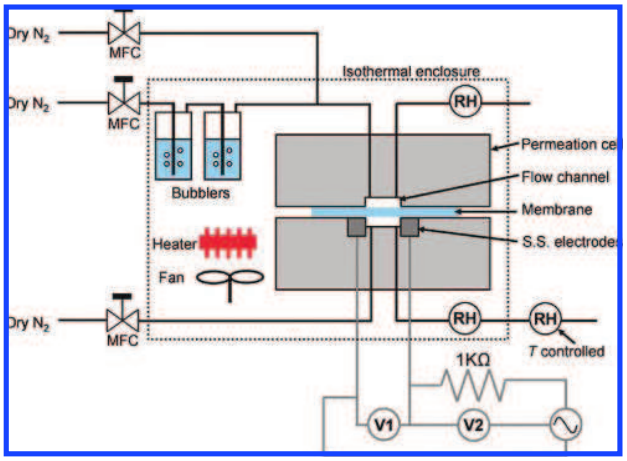

Figure 1. Schematic representation of permeation experiment. The bubblers, permeation cell, and relative humidity sensors were maintained in an isothermal enclosure (dashed line) during experiments. One relative humidity sensor, on the dry side exit, was located outside the isothermal enclosure with independent temperature control.

samples were stored in liquid water at room temperature and installed in the permeation cell fully hydrated. Membranes without gas diffusion layers were installed without using a gasket since the Nafion made a good seal with the permeation cell.

Some of the permeation tests included a carbon GDL on one side of the membrane. For these tests, a woven carbon cloth electrode with microporous layer treated with PTFE wet proofing purchased from E-TEK was used (E-TEK A-6: ELAT, single sided; from E-TEK Division of De Nora N.A., Inc., Somerset, NJ USA). The GDL was applied to a Nafion 115 membrane with the microporous layer in contact with the membrane. An electrode measuring 2.5 cm × 2.5 cm was hot pressed to the membrane at 135 °C using a total force of 8 900 N (average pressure of 1.53 MPa over the entire MEA). The GDL/membrane structure was placed against a square silicone rubber gasket, 7.6 cm on a side with a 1 cm × 1 cm hole in the center cut to fit around the GDL. Hot pressing of the GDL to the membrane was done starting with a fully hydrated Nafion. Preheating took ∼13 min, after which full pressure was applied for 90 s. To improve the adhesion between the electrode and Nafion, a 1/8" thick rubber sheet was placed over the membrane/GDL structure during pressing.

Permeation Instrument. Water permeation was measured through Nafion membranes using a custom-built permeation cell housed in an isothermal enclosure. The permeation cell sandwiched the membrane between two pieces of 2.5 cm thick polycarbonate. Each half of the cell had a square 1 cm^2 × 0.5 cm deep flow channel machined in the center, which had an inlet and outlet through which vapor or gas could flow. The halves were designed to be bolted together with a membrane separating the two flow channels. A maximum operating temperature of ∼100 °C for the cell was based on the upper working temperature of the polycarbonate. The inlet and outlet for each cell half was connected to 1/8" PTFE tubing with a tube-to-female pipe adapter.

Water activity was introduced to the feed flow channel by flowing either liquid water or humidified N_2. N_2 flowed through the dry channel. Figure 1 is a schematic representation of the permeation cell along with controls and instrumentation. (Photographs of the permeation cell can be seen in Chapter 3 of the author's thesis, available on the web at http://pemfc.princeton.edu/theses.html).

The water activity of the N_2 streams exiting both sides of the cell were separately measured using commercially available relative humidity sensors (Sensirion model SHT75) mounted in custom-built housings. The nominal operating range of the humidity sensors was −40 to 124 °C and 10−90% RH. In the nominal operating range the error in RH was ± 3%; outside the nominal range the error in measurement increased to ±10%RH at both extremes. When the water vapor content at the outlet was <10%RH at the cell temperature, an additional relative humidity sensor was installed outside the heated enclosure and temperature controlled to a temperature where the relative humidity was >10%. This provided a more precise measurement of water partial pressure of the gas leaving the permeation cell.

For liquid feeds, a peristaltic pump provided a constant flow of liquid water. The flow rate was kept low (∼5 mL/min) to maintain the liquid pressure at 1 bar. Humidified N_2 feed was supplied by mixing dry and humidified N_2 streams. Nitrogen was passed through two heated bubblers to establish a water activity of ∼0.9. Water activities between 0.00 and 0.9 were obtained by mixing humidified N_2 with dry N_2. The total flow rate of humidified N_2 on the feed side was between 1 and 3 L/min, which ensured that the change in relative humidity between the gas entering and leaving the feed side flow channel was less than 2%.

N_2 flow on the dry side of the cell was accurately maintained by mass flow controllers. For flows between 5 and 50 sccm, an Alborg mass flow controller was used (model GFC 17). For flows between 75 and 1000 sccm, an MKS mass flow controller was used (model 1179 A-13 CR-BV). Bubble meters were used to calibrate the mass flow controllers.

The permeation cell was installed in an isothermal housing consisting of an insulated base and a removable insulated top. A fan (heating duct booster fan) provided forced convection to maintain an isothermal environment. A PID controller controlled the temperature in the chamber. Gas flowed through 25 ft. of coiled metal tubing (1/4" diameter copper for N_2 and 1/8" diameter for liquid water) to bring the temperature of the incoming fluids to that of the chamber.

Humidification bubblers were built from stainless steel tube/pipe and flanges. The bubblers had a total volume of ∼1.5 L, 30−70% filled with liquid water. N_2 entered at the bottom of the bubbler through a frit, creating millimeter sized bubbles that rose through the liquid and collected in the free space at the top of the bubbler. The bubblers were located inside the isothermal chamber, being heated to the temperature of the chamber and eliminating condensation that might otherwise arise from thermal gradients.

Permeation Measurements. Relative humidity of both the feed stream and the effluent of the dry stream were recorded at 1 Hz and logged by computer. The activity of water on the feed side, a_f, (liquid water or humidified nitrogen) was kept nearly constant by using a large excess flow. The water activities at both the inlet and outlet of the feed side were monitored, and the variations in water activity was always <0.01. The water activity leaving the dry side, a_d, was measured as a function of the dry N_2 flow rate. The open cavity flow channel of the permeation cell was designed to provide good mixing; the gas composition of the effluent will be the same as the gas composition in the gas plenum of the permeation cell. This flow channel design permitted us to assume one-dimensional (1D) transport, greatly simplifying the data analysis.

The permeation rate was calculated from the relative humidity, temperature, and flow rate at the exit of the dry side of the

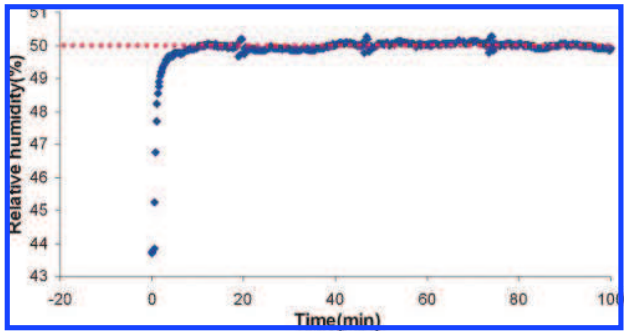

Figure 2. Raw permeation data showing the relative humidity of N_2 exiting the permeation cell at the dry side. The red dashed line indicates the average relative humidity at steady state. Relative humidity was measured at 80 °C for a N1110 membrane with 80%RH vapor on the feed side. The N_2 flow rate at the dry side was decreased from 20 to10 mL/min at $t = 0$.

cell. Relative humidity and temperature were recorded until a steady state value was reached. A representative plot of dry side relative humidity versus time after a change in the nitrogen flow rate is shown in Figure 2. Knowing the cell temperature, T, the dry N_2 flow rate, Q, and relative humidity, RH, in the dry side effluent, the water flux was calculated from eq 1.

$$\text{Flux} = \frac{Q\rho_g}{A_{mem}} \frac{M_V \frac{RH}{100} p_{sat}}{M_g\left(p_{tot} - \frac{RH}{100} p_{sat}\right)} \quad (1)$$

Q is the volume flow rate of dry N_2 at the dry side with density ρ_g, M_V is the molecular weight of water, M_g is the molecular weight of N_2, p_{tot} is the total pressure of the water vapor/gas mixture (assumed to be 1 bar), p_{sat} is the saturation vapor pressure of liquid water at the temperature at which the relative humidity was measured, and A_{mem} is the area of the membrane. The Goff−Gratch equation was used to calculate the saturation vapor pressure of water at temperature T.[25]

1D Permeation. Ideal 1D water permeation through a membrane is illustrated in Figure 3. Water activity outside the membrane in the bulk vapor or liquid phases is a_f and a_d at the feed and dry sides, respectively. Steady state water transport is driven by the water activity gradient. Inside the membrane water transport occurs by diffusion. If the water diffusion coefficient, D, is constant with water activity; the water activity profile across the membrane is linear. If D depends on water activity, the profile is nonlinear. The activity gradients at the membrane's surfaces may be discontinuous due to the phase change between the fluid and membrane. A microscopic interfacial region exists where a combination of diffusion and phase change occur. The thickness and transport properties of this interfacial region are difficult to describe quantitatively; transport across the interfacial region is accounted for by interfacial mass transport coefficients k_f or k_d, at the feed and dry side respectively.

The interfacial mass transport coefficient k accounts for both phase change and gas phase boundary layer at the membrane/vapor interface. At sufficiently high gas velocity the gas phase boundary layer resistance is negligible, and the permeation is independent of gas velocity. When a GDL is place against the membrane, a gas phase boundary layer resistance to transport is always present; the gas flow field does not penetrate the GDL. For a liquid water/membrane interface there is no gas boundary

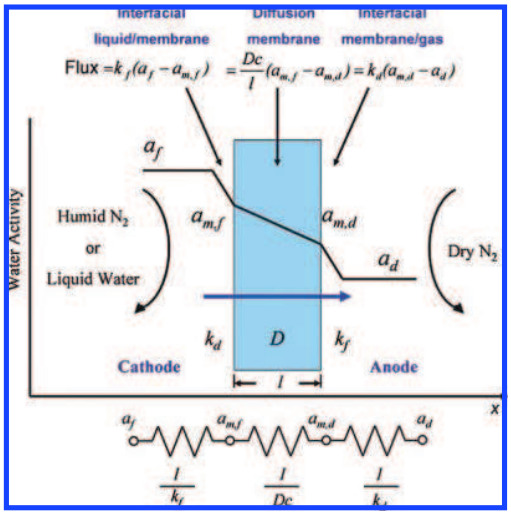

Figure 3. 1D permeation of liquid water or water vapor through a Nafion membrane into dry N_2. Activity profile is shown along with mass transport coefficients. Steady state permeation equations are shown at the top of the figure, and the equivalent network of resistors describing mass transport resistances is shown at the bottom.

layer, and interfacial mass transport resistance is only due to phase change.

There are kinetic barriers associated with transport between phases, for example evaporation/condensation at vapor/liquid interface or solution/dissolution at a liquid/solid interface. The interfacial transport coefficients correlate the observed mass transport across an interfacial boundary to the activity difference between the two macroscopic phases. Water flux into the membrane is given by the difference in water activity between the bulk and the membrane interface according to eq 2,

$$\text{flux} = k_f(a_f - a_{m,f}) \quad (2)$$

A similar expression is obtained for water transport from the membrane into the vapor phase,

$$\text{flux} = k_d(a_{m,d} - a_d) \quad (3)$$

Water flux through the membrane is the result of diffusion. If the diffusion coefficient is independent of concentration, then the flux across the membrane is given by eq 4.

$$\text{flux} = \frac{Dc}{l}(a_{m,f} - a_{m,d}) \quad (4)$$

Here, c is the standard state concentration of water in the membrane and l is the membrane thickness.

The overall mass transfer coefficient k_o or permeability describes the net water flux based on the difference in water activity between the bulk fluid at the feed side and dry side of the membrane (eq 5). The overall mass transfer coefficient, k_o, is experimentally determined; values for diffusion coefficients and interfacial transport are all based on models of how k_o is dependent on concentration.

$$\text{flux} = k_o(a_f - a_d) \quad (5)$$

Mass conservation dictates that, at steady state, the flux into and out of the membrane is equal to the flux through the membrane. As such, eq 2−5 can be related to the overall flux.

$$\text{flux} = k_o(a_f - a_d) = k_f(a_f - a_{m,f}) = \frac{Dc}{l}(a_{m,f} - a_{m,d}) = k_d(a_{m,d} - a_d) \quad (6)$$

Permeation through a membrane is shown in Figure 3 with mass transport resistances due to interfacial transport and diffusion included. Since these mass transport resistances are in series, the overall mass transport resistance can be related to the individual components where k_o can be expressed in terms of the interfacial transport coefficients and the membrane diffusivity.

$$k_o = \frac{\frac{Dc}{l}k_d k_f}{\frac{Dc}{l}k_d + \frac{Dc}{l}k_f + k_d k_f} \quad (7)$$

Equation 7 is useful for indentifying the controlling resistance to water transport. If diffusion is the limiting resistance for mass transport, then $Dc/l \ll k_d$, k_f and $k_o = Dc/l$. When diffusion is the limiting resistance the permeation rate should decrease inversely with membrane thickness. In contrast, if interfacial mass transport is the limiting resistance then the permeation rate should be independent of membrane thickness.

Results

Liquid Water Permeation. Permeation of water through Nafion membranes of three different thicknesses at 30 and 80 °C with the liquid water at the feed side is shown in Figure 4. Water flux is nearly independent of membrane thickness at both 30 and 80 °C for membranes from 51 to 254 μm thick. These data suggest that when liquid water is present on the feed side of the membrane the transport of water across the membrane is limited by interfacial transport at the membrane−vapor interface.

The water flux increased from 30 to 80 °C for all membrane thicknesses. Comparing Figures 4A and 4B, it is also apparent that the limiting water flux was achieved at lower N_2 flow rates at 80 °C than at 30 °C. The limiting flux is achieved when the permeation rate is fast compared to the residence time, τ, for gas flow through the permeation cell, $k_o > \tau = Q\rho_g M_V/A_{mem}M_g$. A semiquantitative analysis of Figures 4A and 4B indicates that the overall permeation coefficient increases by approximately a factor of 4 between 30 and 80 °C. The permeation rate as a function of N_2 flow rate can be fit to eq 8, to determine the overall permeation coefficient. Equation 8 equates the experimental flux from eq 1 to the permeation rate given in eq 5.

$$k_o(a_f - a_d) = \frac{Q\rho_g}{A_{mem}}\frac{M_V(a_d)}{M_g(1 - a_d)} \quad (8)$$

Permeation measurements at 50 and 70 °C were qualitatively identical to those presented in Figure 4; permeation rates increased with temperature from 30 to 80 °C. At all temperatures, water permeation rates from liquid water through Nafion N115 (127 μm) and N1110 (254 μm) were essentially identical. A summary of the limiting water permeation from liquid water through Nafion at high dry N_2 flow rate is given in Table 1.

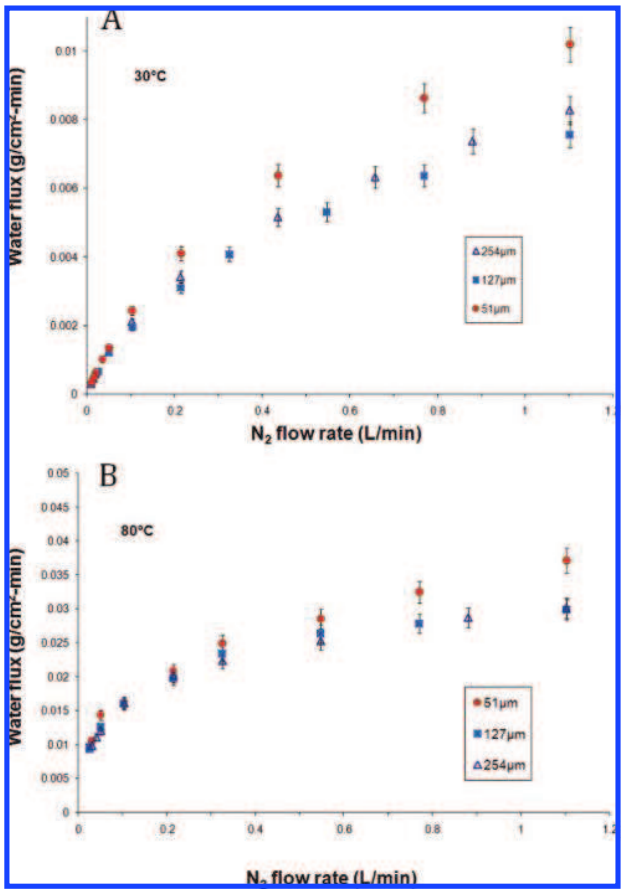

Figure 4. Comparison of membrane thickness for permeation of liquid water. (A) 30 °C. (B) 80 °C.

TABLE 1: Summary of Water Flux through Nafion[a]

membrane	temperature (°C)	flux at 1.1 L/min (g/cm²·min)
N112	30	0.010
	50	0.023
	70	0.041
	80	0.037
N115	30	0.0076
	50	0.017
	70	0.027
	80	0.030
N1110	30	0.0083
	50	0.015
	70	0.024
	80	0.030

[a] Liquid Water at Feed.

Water Vapor Permeation. Water permeation through Nafion N1110 at 30 and 80 °C for three feed side water activities is shown in Figure 5. The fluxes with water vapor on the feed side of the membrane are an order of magnitude less than the water flux from liquid water. The water flux increases with feed side water activity and with temperature. Comparing Figures 4 and 5 it is evident that the permeation rate reached its plateau value at lower N_2 flow rates when the feed side was water vapor than liquid water. Permeation of water through Nafion membranes of different thicknesses is shown in Figure 6 for feed side water activities of 0.3 and 0.8 at 80 °C. The flux decreases inversely proportional to the membrane thickness. The limiting fluxes as functions of membrane thickness, temperature, and feed side water activity are summarized in Table 2. At 30 °C

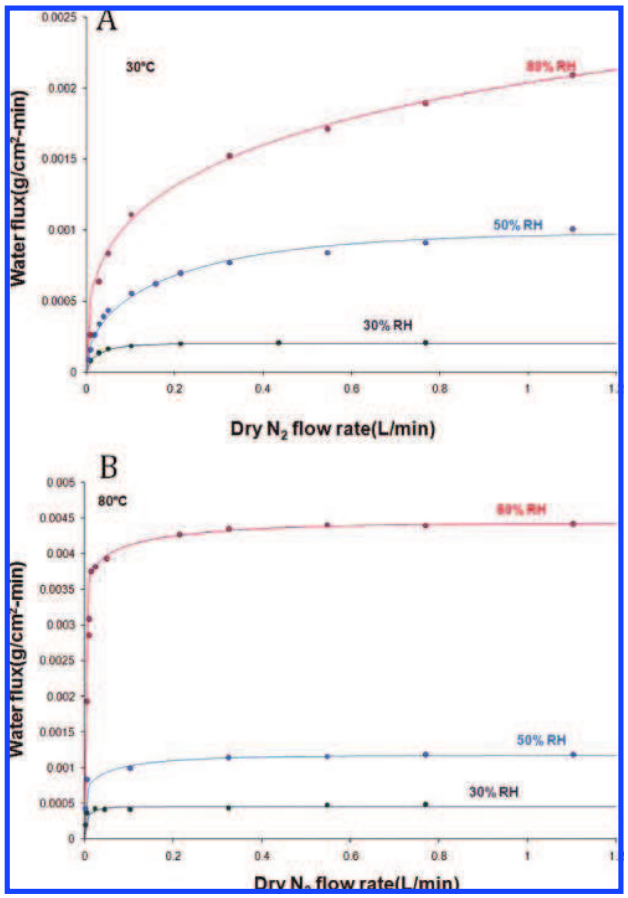

Figure 5. Permeation of water vapor through Nafion N1110 into dry N_2 with the water activity at the feed side at the levels indicated. (A) 30 °C. (B) 80 °C.

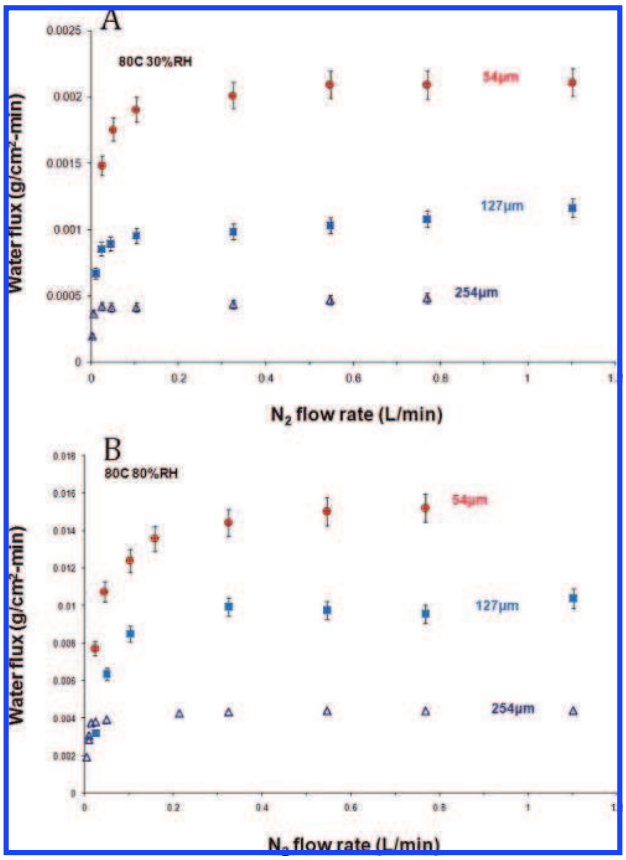

Figure 6. Comparison of water permeation from water vapor at 80 °C with membrane thickness indicated. (A) Feed side water activity $a_w = 0.3$. (B) Feed side water activity $a_w = 0.8$.

the limiting water flux through N1110, N115, and N112 membranes scaled by the ratio of 1:2.9:4.1; this ratio is close to the inverse ratio of the dry membrane thicknesses, 1:2.5:5. This suggests that diffusion is the predominant resistance to water transport at these conditions.

Water Permeation Coefficient. The permeation coefficient is equal to the water flux normalized by the water activity across the membrane, as defined by eq 9.

$$\text{Flux}_{\text{Normalized}} = \frac{\text{Flux}}{(a_f - a_d)} = k_o \qquad (9)$$

Figure 7 shows the permeation coefficient for Nafion 1110 increases as the feed side water activity at 30, 50, 70, and 80 °C. The permeation coefficient increases linearly with water activity from $0 < a_f < 0.9$; there is a large jump in permeation coefficient between $a_f = 0.9$ and 1.0.

Figure 8 tracks the permeation coefficient at 80 °C for membranes of different thicknesses. Permeation coefficients increased with feedwater activity for all three membrane thicknesses. Permeation coefficients are slightly greater for the thinnest membrane (N112), whereas the thicker membranes, N115 and N1110, have nearly identical permeation coefficients.

The sharp increase in permeation coefficient at high feedwater activity appears to be correlated with water absorption by Nafion. The water uptake by Nafion as a function of water activity[26] has been plotted in Figure 8. The water uptake, λ, is the normalized moles of water absorbed per moles of sulfonic acid in the membrane.

Permeation Including Gas Diffusion Layer. Water permeation through Nafion 115 with a porous carbon gas diffusion layer (GDL) on only one side was measured at 30 and 80 °C. Water flux was measured for vapor feeds with activities of 0.3, 0.5, and 0.8 as well as for liquid feeds. A comparison was made between membranes which had the GDL on either the feed side or the dry side. The effect on the permeation coefficient of having the GDL on either side of the membrane is summarized in Figure 9. The GDL reduced the water flux. The effect of the GDL layer was approximately the same on both sides of the membrane; the permeation rate was reduced by 20−50% compared to the bare membrane.

The results for the steady state water flux through Nafion 115 with a gas diffusion layer on one side of the membrane are summarized in Table 3. The permeation rates reported are the limiting flux obtained at the highest nitrogen flow on the dry side of the membrane. More detailed results from permeation measurements at lower flow rates are available from Paul Majsztrik's thesis, available on our Web site (http://pemfc.princeton.edu/theses.html/).

Discussion

Water permeation across Nafion membranes is not consistent with simple diffusion models that have been commonly assumed in the literature.[11,14−16] The key results may be summarized as:

1. The water permeation coefficient of Nafion increases as a function of the membrane water content.

TABLE 2: Water Diffusivity in Nafion Membranes from a Microphase Separated Model

temperature (°C)	membrane thickness (mm)	feed water activity	linear expansion coefficient	measured water flux (g/min)	water diffusivity × 10^6 (cm^2/s)
30	51	0.3	0.03	8.20×10^{-4}	1.59
30	51	0.5	0.045	1.65×10^{-3}	1.45
30	51	0.8	0.075	3.92×10^{-3}	1.59
30	51	1.0	0.20	1.00×10^{-2}	1.68
30	127	0.3	0.03	5.74×10^{-4}	2.76
30	127	0.5	0.045	1.05×10^{-3}	2.29
30	127	0.8	0.075	2.72×10^{-3}	2.75
30	127	1.0	0.20	7.60×10^{-3}	3.19
30	254	0.3	0.03	2.00×10^{-4}	1.93
30	254	0.5	0.045	4.43×10^{-4}	1.93
30	254	0.8	0.075	2.13×10^{-3}	4.30
30	254	1.0	0.20	8.30×10^{-3}	6.96
80	51	0.3	0.03	2.08×10^{-3}	4.02
80	51	0.5	0.045	5.52×10^{-3}	4.84
80	51	0.8	0.075	1.50×10^{-2}	6.08
80	51	1.0	0.20	3.70×10^{-2}	6.23
80	127	0.3	0.03	1.14×10^{-3}	5.49
80	127	0.5	0.045	2.85×10^{-3}	6.22
80	127	0.8	0.075	9.88×10^{-3}	9.97
80	127	1.0	0.20	3.00×10^{-2}	12.6
80	254	0.3	0.03	4.50×10^{-4}	4.33
80	254	0.5	0.045	1.17×10^{-3}	5.11
80	254	0.8	0.075	4.43×10^{-3}	8.94
80	254	1.0	0.20	3.00×10^{-2}	25.1

2. At feed side water activity <0.8, the permeation coefficient scales inversely with membrane thickness. At feedwater activity of 1.0 the water permeation rate was independent of membrane thickness.

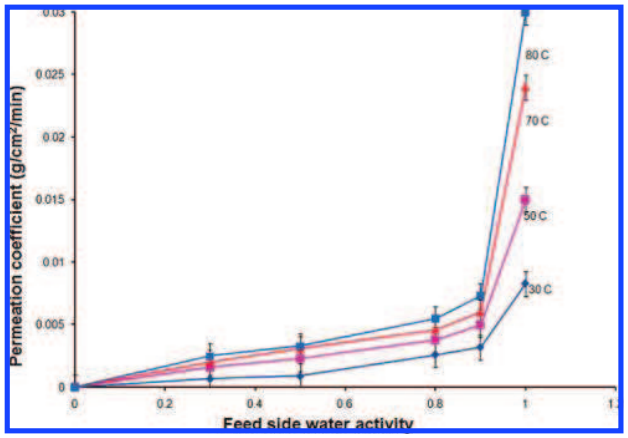

Figure 7. Water Permeation coefficient through Nafion 115 membranes as a function of feed side water activity and temperature.

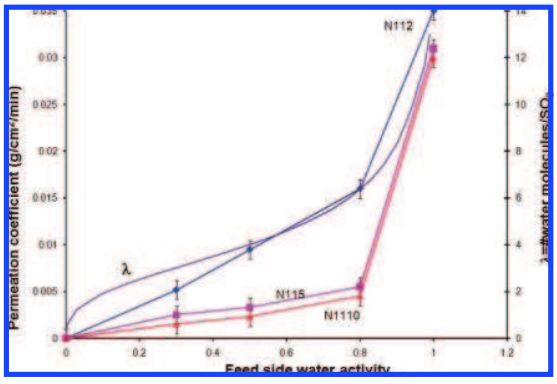

Figure 8. Permeation coefficients for N112, N115, and N1110 at 80 °C as functions of the feed side water activity. Also shown is the water uptake, λ, by 1100 equivalent weight Nafion at 80 °C.

3. A gas diffusion layer reduces the permeation rate by approximately 50%.

The results show that water permeation depends on membrane thickness, membrane water content, temperature, and the feed side water activity. A surprising result was that the water permeation rate was nearly independent of membrane thickness when liquid water was present at the feed side of the membrane. We previously suggested that the permeation was limited by water transport across the interfacial polytetrafluoroethylene (PTFE) layer at the Nafion/gas interface.[1] Several experimental studies have found that exposure of a Nafion surface to liquid water appears to change it from hydrophobic to hydrophilic.[27−29] Weber and Newman suggested that a change in the surface composition might affect water transport in PEM fuel cells.[30] The experiments reported here coupled with our studies of the mechanical properties of Nafion at elevated water activities[7,31] provide a more refined explanation of this result. We suggest that water is transported only through the hydrophilic domains of Nafion. Water absorption swells hydrophilic domains in

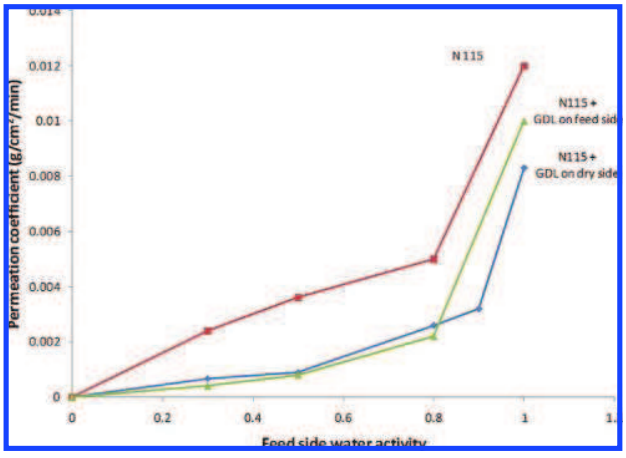

Figure 9. Permeation coefficient for water transport through a Nafion 115 membrane at 30 °C with a gas diffusion layer on either the feed side or dry side of the membrane.

TABLE 3: Summary of Permeation through Nafion N115 with a Carbon Cloth Electrode[a]

GDL location	temperature (°C)	feed side water activity	water flux (g/cm^2/min)	Δa_w across the GDL*
feed side	30	0.3	0.00030	0.022
		0.5	0.00061	0.045
		0.8	0.00097	0.072
		1	0.0017	0.12
	80	0.3	0.0012	0.007
		0.5	0.0028	0.016
		0.8	0.0070	0.041
		1	0.012	0.071
dry side	30	0.3	0.00004	0.003
		0.5	0.00015	0.011
		0.8	0.00064	0.047
		1	0.0020	0.147
	80	0.3	0.00014	0.001
		0.5	0.00040	0.002
		0.8	0.0018	0.011
		1	0.010	0.059

[a] Flux is reported at a dry side N_2 flow rate of 1.1L/min.

Nafion, increasing the volume available for water transport, hence increasing the permeation coefficient. At the highest water activities (feed side water activity approaching 1) the transport through the membrane becomes fast, and the limiting transport resistance is an interfacial resistance at the membrane/gas interface.

Diffusion with Dimensional Change. Nafion is a microphase separated polymer; the phase separation is driven by the interaction energy between the constituent groups. The tetrafluoroethylene backbone and perfluoroether side chain have similar solubility parameters (13.6 and 13.9 (J/cm^3)$^{1/2}$, respectively)[32] and will by miscible, forming a continuous hydrophobic phase. The sulfonic acid groups and water have much larger solubility parameters (33 and 48 (J/cm^3)$^{1/2}$, respectively)[32] and will separate into a hydrophilic phase. Water transport will occur through both the Teflon-like hydrophobic phase and the hydrophilic phase containing the sulfonic acid groups and water. The phases should be bicontinuous with percolation paths that extend across the membrane. The permeation coefficient in each phase is the product of the diffusion coefficient and the concentration (or solubility) in each phase. The water solubility in PTFE is <0.05 wt %.[33] The water solubility in the SO_3H hydrophilic phase at $\lambda = 12$ is 68 wt %. Since the concentration of water in the hydrophobic phase is negligible, the contribution of water transport in the hydrophobic phase is negligible; water transport is only through the hydrophilic phase.

Water is also absorbed into the hydrophilic phase of Nafion, causing it to swell and increase the volume through which water diffusion occurs, as illustrated in Figure 10. The fractional volume change of the hydrophilic phase is much greater than the overall fractional volume change of the Nafion. In the absence of absorbed water, the volume fraction of the hydrophilic domain, φ_o, is the volume fraction of the sulfonic acid groups. Assuming sulfonic acid groups (SO_3H) are the same size as sulfuric acid molecules, $\varphi_o = (\rho_{Nafion} M_{w,SO_3})/(E_W \rho_{SO_3})$, where ρ_{Nafion} is the density of dry Nafion (2 g/cm^3), ρ_{SO_3} is the density of SO_3 (1.8 g/cm^3), M_w is the molecular weight of SO_3, and E_W is the equivalent weight of Nafion (grams of polymer per mole of sulfonic acid groups). For Nafion N1100, φ_o is 0.08. Water absorption increases the volume of Nafion by an amount $\Delta V/V_o = ((1 + \varepsilon(a_w))^3 - 1)$ where V_o is the initial volume of dry membrane and $\varepsilon(a_w)$ is the linear expansion coefficient of Nafion due to absorption of water. This volume change is

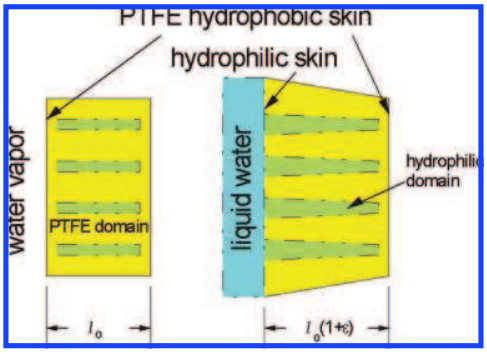

Figure 10. Expansion of hydrophilic domains of Nafion by water absorption. A 10% linear expansion produces a 100% increase in the area for water transport. The figure also illustrates how the surface is hydrophobic when contacting vapor, but liquid water draws the hydrophilic domains to the surface, thereby reducing the interfacial transport resistance for water.

entirely associated with the hydrophilic phase; the volume of the hydrophobic remains constant. (The hydrophobic phase may be deformed by swelling of the hydrophilic phase, but its volume will be conserved). As a result of water absorption, the volume of the hydrophilic phase, which is available for water transport, increases from $V_o\varphi_o$ to $(V_o\varphi_o + \Delta V)$. The water flux in the Nafion membrane is given by eq 10. Equation 10 is an extension of eq 4, where the volume-averaged standard state concentration and diffusivity, c and D, have been replaced by c'_o and D', which refer to the standard state concentration and diffusivity of water in the hydrophilic phase. The factor A_T/A_{mem} accounts for the hydrophilic phase areal fraction of the membrane of the membrane available for water transport.

$$\text{flux} = \frac{A_T}{A_{mem}} c'_o D' \frac{\partial a_w}{\partial x} \tag{10}$$

Assuming water is only absorbed into the hydrophilic phase, the effective areal fraction for water transport as a function of water activity is given by eq 11,

$$\frac{A_T}{A_{mem}} = \frac{(V_o\varphi_o + \Delta V)/l_o(1 + \varepsilon(a_w))}{V_o(1 + \varepsilon(a_w))^3/l_o(1 + \varepsilon(a_w))} = \frac{\varphi_o + [(1 + \varepsilon(a_w))^3 - 1]}{(1 + \varepsilon(a_w))^3} \tag{11}$$

where l_o is the dry membrane thickness. The standard state concentration of water in the hydrophilic phase (the concentration of water at water activity of unity) is given by the mass of water divided by the volume of the hydrophilic phase when Nafion is equilibrated with liquid water. The standard state concentration of water is given by eq 12 (where $\varepsilon_m = 0.2$ is the linear expansion coefficient of Nafion in liquid water).

$$c_o = \frac{[(1 + \varepsilon_m)^3 - 1]\rho_w}{\varphi_o + [(1 + \varepsilon_m)^3 - 1]} \tag{12}$$

The linear expansion coefficient of Nafion as a function of water activity is plotted in Figure 11, and the values are summarized in Table 2.[31] Combining the flux measurements with the linear

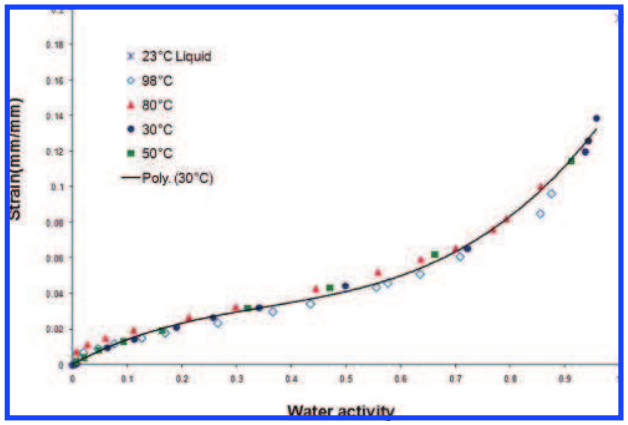

Figure 11. Linear strain of 1100 equivalent weight Nafion as a function of water activity. The data were taken at different temperatures with water vapor activity controlled. The point in the upper right corner is from liquid water at 23 °C.

expansion coefficient values the diffusion coefficients of water through Nafion has been estimated using eq 13 and assuming a linear gradient in water activity across the membrane; the diffusion coefficient values are summarized in Table 2.

$$D \approx \frac{A_{mem}}{A_T}\frac{(\text{flux})l_o(1+\varepsilon)}{c_o(\Delta a_w)} = \frac{(\text{flux})l_o}{(\Delta a_w)A_o c_o}\frac{(1+\varepsilon)^3}{[\varphi_o + (1+\varepsilon)^3 - 1]} \quad (13)$$

Previous studies using permeation to determine water diffusion in Nafion treated Nafion as a homogeneous system.[11,14−16] That assumption overestimated the volume available for water transport, resulting in diffusion coefficients that were an order of magnitude smaller than those shown in Table 2. Furthermore, the diffusion coefficients determined in those studies suggested the diffusion coefficients increased by more than a factor of 10 with increasing water activity. Accounting for water transport only in the hydrophilic phase gives diffusion coefficients that show a much weaker dependence on water activity. The diffusion coefficients are also in much closer agreement with the self-diffusion coefficients determined by NMR.[5,10−13] The diffusion coefficients determined with eq 13, like those determined by NMR, show weak dependence on the water activity, as can be seen in Table 2.

Several models for water transport in Nafion have suggested that the polymer consists of a network of hydrophilic pores and water transport is hydraulically driven by capillary forces.[30,34−37] This requires the existence of a vapor/liquid interface, corresponding to high water activities. The driving force for the water flux is the gradient in capillary pressure, P_c, in the hydrophilic pores, and the transport coefficient is a Darcy's law permeability, K, as shown in eq 10a.

$$\text{flux} = \frac{A_T}{A_{mem}}K\frac{\partial P_c}{\partial x} \quad (10a)$$

The flux driven by the capillary pressure will still increase due to the increased areal fraction of the hydrophilic phase available for transport.

Equations 10−13 assume that water is only transported through the hydrophilic phase and the volume of the hydrophilic phase changes due to water absorption. Our analysis has assumed that water is transported through the membrane by diffusion. The volume of the hydrophilic phase increases from 0.08 at $a_w = 0$ to 0.47 at $a_w = 1.0$. This 6-fold increase in volume is a geometric effect that results in water transport increasing by the same amount. The permeation data are consistent with a constant diffusivity, and the change in flux was principally due to a change in the hydrophilic volume through which water diffusion occurred. Other factors are also expected to impact the water transport. Structural changes in the microphases that alter the connectivity of the hydrophilic phase and chemical changes associated with the hydration state of the sulfonic acid groups are also expected to affect the diffusivity of water.[38] The pore network of hydrophilic pores might also sustain osmotic pressures. We anticipate these to affect water transport, but the analysis presented here suggests that they are less important than the geometric effect of increasing the volume of the hydrophilic phase.

Interfacial Transport. The most perplexing result from the permeation studies is why does the permeation coefficient appear to approach a constant value that is almost independent of membrane thickness at the highest water activity? This result suggests that water transport is limited by interfacial transport at high water activity. It has been suggested that a Teflon-like surface is at the vapor/membrane interface.[1,9,27,30] Recent experimental studies of surface wetting have confirmed this model.[29] The surface of Nafion is hydrophobic when exposed to a vapor (even a humidified vapor) and switches to hydrophilic when contacted with liquid water. The hydrophobic surface is Teflon-like skin through which water must move. The mass transfer coefficient, k_m, across a thin Teflon-like film can be estimated from the water solubility in Teflon, the diffusivity, and the film thickness (~1 nm) as shown in eq 14.

$$k_m \approx \frac{c_{w,teflon}D_{w,teflon}}{l_{teflon\ layer}} \approx \frac{(10^{-7}\ \text{g/cm}^3)(10^{-4}\ \text{cm}^2/\text{min})}{(10^{-8}\ \text{cm})} \sim 10^{-3}\ \text{g/cm}^2\cdot\text{min} \quad (14)$$

This estimate of the interfacial mass transport resistance is of the same order of magnitude as the overall water permeation coefficient.

The limiting resistance for water permeation will depend on the interfacial transport resistance and diffusion, as suggested by eq 7. However, eq 7 should be modified to account for the change in diffusional resistance with water activity because of the increased volume of the hydrophilic domains. Accounting for the interfacial resistance of the hydrophobic Teflon-like layer and the volume change of the hydrophilic regions, the overall mass transport coefficient is given by eq 15.

$$k_o = \frac{\frac{D_{w,hydrophilic}c_m}{l_{Nafion}}\frac{\varphi}{\varphi_o}k_m}{\frac{D_{w,hydrophilic}c_m}{l_{Nafion}}\frac{\varphi}{\varphi_o} + k_m} \quad (15)$$

At $a_w \le 0.8$, $\varphi/\varphi_o < 2.5$ and the diffusion of water through the Nafion is the limiting transport resistance. As $a_w \rightarrow 1$, $\varphi/\varphi_o \rightarrow$

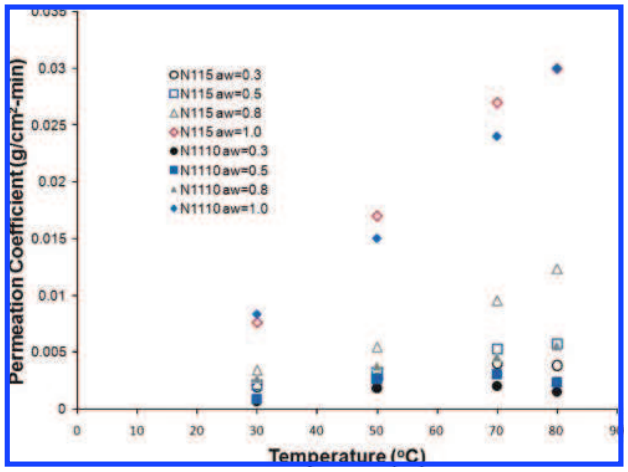

Figure 12. Water permeation coefficients through Nafion 115 and Nafion 1110 as functions of temperature and water activity.

10, and the interfacial transport resistance across the Teflon-like film becomes the limiting transport resistance.

Both temperature and film thickness also play a role in determining which transport resistance is limiting. If the Nafion film were thicker, $l_{Nafion} > 1$ mm, then even at the high water activities diffusion would be the limiting resistance. Interfacial mass transport is also more temperature sensitive than diffusion. The permeation coefficient of water as a function of temperature is plotted as a function of water activity in Figure 12. At the highest water activity, where interfacial transport is rate limiting, the permeation coefficient has a much stronger temperature dependence than that at low water activities. We suggest that this could be due to increased water solubility in the Teflon-like layer at higher temperature. At the low water activities, where diffusion is the limiting transport resistance, the permeation shows little sensitivity to temperature.

Effect of Gas Diffusion Layer on Permeation. In fuel cell applications the membrane itself is not in direct contact with the gas streams in the flow channels. There are porous GDLs that serve to carry electrical current that separates the membrane from the gas flow channel. The porous GDLs create an additional transport resistance to transport, affecting the overall permeation. Permeation results with a GDL included (Figure 9), show that the permeation coefficient was diminished by approximately 20−50% relative to a bare membrane. Water vapor transport across the GDL can be approximated by diffusion through a porous media and is expected to scale linearly with water activity difference across the porous layer. The water activity gradient across the GDL can be estimated based on a simple linear diffusion model across the layer. The activity difference across the GDL, Δa, should be well-approximated by eq 16, where D_g is the diffusivity of water vapor in air ($D_g = 0.212 + 1.5 \times 10^{-3}$ T·cm^2/s), c_o is the standard state concentration of water vapor ($c_o = P_w^{\circ}/RT$), F is the water flux, and l_{GDL} is the thickness of the GDL (0.035 cm).

$$\Delta a = \frac{F l_{GDL}}{D_g c_o} \qquad (16)$$

The water activity across the GDL was calculated based on eq 16, and the results are summarized in Table 3. Typically, the water activity difference across the GDL was <10% of the total activity difference between the feed side and the dry side. This is confirmation about the assumption that the GDL is a small contribution to the overall resistance to water transport in PEM fuel cells.

Conclusions

Water permeation through Nafion increases with feed side water activity, rising rapidly at high water activities. The permeation rate becomes independent of membrane thickness at high feed side water activity. It was shown that the permeation data is consistent with water diffusion through the hydrophilic phase of microphase-separated Nafion. The volume for water transport in the hydrophilic phase increases due to water absorption, which permits higher transport rates. This geometric factor accounts for a 10-fold increase of the apparent diffusion coefficient as a function of water activity. At high water activity water transport is limited by interfacial mass transport at the membrane/gas interface.

Acknowledgment. The authors thank the National Science Foundation (CTS- 0354279 and DMR-0213707 through the Materials Research and Science Engineering Center at Princeton) for support of this work.

References and Notes

(1) Majsztrik, P. W.; Satterfield, M. B.; Benziger, J.; Bocarsly, A. B. *J. Membr. Sci.* **2007**, *301*, 93–106.
(2) Ge, S. H.; Li, X. G.; Yi, B. L.; Hsing, I. M. *J. Electrochem. Soc.* **2005**, *152*, A1149−A1157.
(3) Thampan, T.; Malhotra, S.; Tang, H.; Datta, R. *J. Electrochem. Soc.* **2000**, *147*, 3242–3250.
(4) Weber, A. Z.; Newman, J. *AIChE J.* **2004**, *50*, 3215–3226.
(5) Zawodzinski, T. A.; Derouin, C.; Radzinski, S.; Sherman, R. J.; Smith, V. T.; Springer, T. E.; Gottesfeld, S. *J. Electrochem. Soc.* **1993**, *140*, 1041–1047.
(6) Doyle, M.; Rajendaran, G. In *Fuel Cell Technology and Applications*; Vielstich, W., Gasteiger, H. A., Lamm, A., Eds.; Wiley: New York, 2003; Vol. 3.
(7) Satterfield, M. B., Mechanical and Water Sorption Properties of Nafion and Composite Nafion/Titanium Dioxide Membranes for Polymer Electrolyte Membrane Fuel Cells. Ph.D. Thesis, Princeton University, 2007.
(8) Yeo, S. C.; Eisenberg, A. *J. Appl. Polym. Sci.* **1977**, *21*, 875–898.
(9) Satterfield, M. B.; Benziger, J. B. *J. Phys. Chem. B* **2008**, *112*, 3693–3704.
(10) Zawodzinski, T. A.; Neeman, M.; Sillerud, L. O.; Gottesfeld, S. *J. Phys. Chem.* **1991**, *95*, 6040–6044.
(11) Hietala, S.; Maunu, S. L.; Sundholm, F. *J. Polymer Sci. Part B-Polymer Phys.* **2000**, *38*, 3277–3284.
(12) Tsushima, S.; Teranishi, K.; Hirai, S. *Energy* **2005**, *30*, 235–245.
(13) Suresh, G.; Pandey, A. K.; Goswami, A. *J. Membrane Sci.* **2006**, *284*, 193–197.
(14) Rivin, D.; Kendrick, C. E.; Gibson, P. W.; Schneider, N. S. *Polymer* **2001**, *42*, 623–635.
(15) Ye, X. H.; LeVan, M. D. *J. Membrane Sci.* **2003**, *221*, 147–161.
(16) Villaluenga, J. P. G.; Barragan, V. M.; Seoane, B.; Ruiz-Bauza, C. *Electrochim. Acta* **2006**, *51*, 6297–6303.
(17) Takamatsu, T.; Hashiyama, M.; Eisenberg, A. *J. Appl. Polymer Sci.* **1979**, *24*, 2199–2220.
(18) Morris, D. R.; Sun, X. D. *J. Appl. Polymer Sci.* **1993**, *50*, 1445–1452.
(19) Hinatsu, J. T.; Mizuhata, M.; Takenaka, H. *J. Electrochem. Soc.* **1994**, *141*, 1493–1498.
(20) Krtil, P.; Trojanek, A.; Samec, Z. *J. Phys. Chem. B* **2001**, *105*, 7979–7983.
(21) Choi, P.; Jalani, N. H.; Datta, R. *J. Electrochem. Soc.* **2005**, *152*, E123−E130.
(22) Jalani, N. H.; Datta, R. *J. Membrane Sci.* **2005**, *264*, 167–175.
(23) Burnett, D. J.; Garcia, A. R.; Thielmann, F. *J. Power Sources* **2006**, *160*, 426–430.
(24) Legras, M.; Hirata, Y.; Nguyen, Q. T.; Langevin, D.; Metayer, M. *Desalination* **2002**, *147*, 351–357.
(25) Goff, J. A.; S., G. *Trans. Am. Soc. Heating Ventilating Eng.* **1946**, 95–122.
(26) Yang, C.; Srinivasan, S.; Bocarsly, A. B.; Tulyani, S.; Benziger, J. B. *J. Membr. Sci.* **2004**, *237*, 145–161.

(27) Zawodzinski, T. A.; Gottesfeld, S.; Shoichet, S.; McCarthy, T. J. *J. Appl. Electrochem.* **1993**, *23*, 86–88.
(28) McLean, R. S.; Doyle, M.; Sauer, B. B. *Macromolecules* **2000**, *33*, 6541–6550.
(29) Goswami, S.; Klaus, S.; Benziger, J. *Langmuir* **2008**, *24*, 8627–8633.
(30) Weber, A. Z.; Newman, J. *J. Electrochem. Soc.* **2003**, *150*, A1008−A1015.
(31) Majsztrik, P. W., Mechanical and Transport Properties of Nafion for PEM Fuel Cells: Temperature and Hydration Effects. Ph.D. Thesis, Princeton University, 2008.
(32) Van Krevelen, D. W. *Properties of Polymers*, 3rd ed.; Elsevier: New York, 1990.
(33) Sperati, C. In *Handbook of Plastic Materials and Technology*; Rubin, I., Ed.; Wiley: New York, 1990; p 117−136.
(34) Divisek, J.; Eikerling, M.; Mazin, V.; Schmitz, H.; Stimming, U.; Volfkovich, Y. M. *J. Electrochem. Soc.* **1998**, *145*, 2677–2683.
(35) Eikerling, M.; Kharkats, Y. I.; Kornyshev, A. A.; Volfkovich, Y. M. *J. Electrochem. Soc.* **1998**, *145*, 2684–2699.
(36) Eikerling, M.; Kornyshev, A. A.; Stimming, U. *J. Phys. Chem. B* **1997**, *101*, 10807–10820.
(37) Bernardi, D. M.; Verbrugge, M. W. *J. Electrochem. Soc.* **1992**, *139*, 2477–2491.
(38) Choi, P. H.; Datta, R. *J. Electrochem. Soc.* **2003**, *150*, E601−E607.

JP804197X